Journal of Solid State Chemistry **160,** 222–229 (2001)
doi:10.1006/jssc.2001.9226, available online at http://www.idealibrary.com on IDEAL®

Molecular Dynamics Simulation of Structural Phase Transitions in $RbNO_3$ and $CsNO_3$

Jianjun Liu,*,[1] Chun-gang Duan,† M. M. Ossowski,* W. N. Mei,†
R. W. Smith,‡ and J. R. Hardy*

*Department of Physics and Center for Electro-Optics, University of Nebraska, Lincoln, Nebraska 68588-0111; †Department of Physics, University of Nebraska, Omaha, Nebraska 68182-0266; and ‡Department of Chemistry, University of Nebraska, Omaha, Nebraska 68182-0109

Received January 12, 2001; in revised form April 18, 2001; accepted April 30, 2001

Structural phase transitions in $RbNO_3$ and $CsNO_3$ are studied by molecular dynamics. The simulations are based on the parameter-free potentials calculated from the Gordon–Kim modified electron gas formalism, extended to ionic molecular crystals. The microscopic mechanism of the structural phase transitions in $RbNO_3$ and $CsNO_3$ is revealed. It is found that the phase IV–III transition in $RbNO_3$ and the phase II–I transition in $CsNO_3$ are initiated by the in-plane and out-of-plane rotations of the NO_3 ions, and the phase III–II–I transitions in $RbNO_3$ are due to dilation along a trigonal axis of phase III, giving phase II a rhombohedral structure. © 2001 Academic Press

Key Words: **molecular dynamics; Gordon–Kim potential; nitrate; phase transition; order–disorder.**

INTRODUCTION

Alkali nitrates are an interesting chemical group that has attracted much attention because each of the alkali nitrates has a different phase diagram. The structures of $RbNO_3$ and $CsNO_3$ are the most complex among the alkali nitrates. At room temperature, $RbNO_3$(IV) and $CsNO_3$(II) have the same trigonal structure with space group $P3_1$ (1, 2). The Rb(Cs) atoms form a pseudocubic sublattice with nine pseudocubes per unit cell. The NO_3 groups are closely planar and each is enclosed by a pseudocube of Rb(Cs) atoms.

At atmospheric pressure, $RbNO_3$ exhibits three polymorphic phase transitions: $IV^{437K} \rightarrow III^{492K} \rightarrow II^{564K} \rightarrow I$ (3). $RbNO_3$(III) is cubic and CsCl-like with orientational disorder of the NO_3 ions (4). $RbNO_3$(I) has been reported to have a f.c.c. lattice which was suggested as having the Rb atoms and NO_3 groups forming a NaCl-type cation–anion arrangement (5, 6). There are some controversies about the structure of $RbNO_3$(II). Three different suggestions were reported, i.e., trigonal (6–8), tetragonal (9), and b.c.c. (10).

At 427 K $CsNO_3$(II) undergoes a first-order structural phase transition into a cubic phase $CsNO_3$(I) which was proposed to have a CsCl-type structure similar to that of $RbNO_3$(III) (11).

Although the structural phase transitions in $RbNO_3$ and $CsNO_3$ have been studied by many experiments, and the IV–III transition in $RbNO_3$ and the II–I transition in $CsNO_3$ were suggested to be associated with the rotational disordering of NO_3 ions, questions concerning the mechanisms of the phase transitions remain, especially for the III–II–I transitions in $RbNO_3$. As far as we know, there is no theoretical study at the microscopic level of the phase transitions in $RbNO_3$ and $CsNO_3$ due to their complex structure.

In this paper we investigate the phase transitions in $RbNO_3$ and $CsNO_3$ by molecular dynamics simulation using parameter-free potentials. Our method starts from quantum-chemistry calculations for the whole NO_3 molecular ion to obtain the optimized structure and the electron charge distribution, and then describes the covalent intramolecular interactions using Taylor expansions of the molecular ion's energy, and calculates the ionic intermolecular interactions using the Gordon–Kim electron gas model (12). This model leads to a parameter-free description of the potential energy surfaces for ionic molecular crystals (13).

INTER- AND INTRAMOLECULAR POTENTIALS AND STATIC RELAXATION

The nitrates investigated consist of free alkali cations (Rb, Cs) and molecular anions (NO_3). The interactions within the same NO_3 ions are covalent, and those between different NO_3 ions are ionic; thus, we consider the intramolecular and intermolecular interactions separately. A full description of the procedure for obtaining both inter- and

[1]To whom correspondence should be addressed. Fax: 402-472-2879. E-mail: jliu@unlserve.unl.edu.

0022-4596/01 $35.00

intramolecular interaction potentials has been given elsewhere (13). Here we outline the main steps.

As a first approximation, we assume that the intramolecular interactions of the NO_3 ion in crystals are the same as those of the free NO_3 ion. The intramolecular interactions of the free NO_3 ion are described by a harmonic expansion of the energy in terms of its bond lengths, bond angles, and dihedral angles. The structure of the free NO_3 ion was obtained by performing a quantum chemistry structural optimization using the GAUSSIAN94 commercial package (14). The standard 6-31G** basis set was used for N and O atoms. The force constants of the harmonic expansion were also calculated from the GAUSSIAN94.

The short-range pair potentials between different NO_3 ions, and between alkali ions and NO_3 ions, were calculated according to the Gordon–Kim electron gas model (12). The charge density of nitrogen and oxygen atoms was obtained from the whole charge density of the free NO_3 ion in the spirit of a Mulliken population analysis (15). The tabulated charge densities of K^+ and Rb^+ were used (16), while those for Cs^+ were calculated with the software of Liberman *et al.* (17). The long-range Coulomb interactions were calculated using the Mulliken charges of the N and O atoms: specifically, $+0.9917$ for N and -0.6639 for O. The ionic charge for the alkali ions is $+1$.

Using the intramolecular and intermolecular ionic interaction potentials obtained above, we performed static relaxation calculations for $RbNO_3$ and $CsNO_3$ with space group $P3_1$ symmetry constraints. Our relaxation was performed for an infinite lattice by applying periodic boundary conditions, and followed a Newton–Raphson algorithm. The standard technique of the Ewald sum was used in calculating the lattice energy and forces.

The parameters for the relaxed structures of $RbNO_3$(IV) and $CsNO_3$(II) along with the experimental values (1, 2) at room temperature are given in Tables 1 and 2. From these tables, one can see that our relaxed structures are in good agreement with experiment. Specifically, a total of 47 parameters for $RbNO_3$ and $CsNO_3$ depend explicitly on the accuracy of the potentials. Almost all of them are reproduced to within a few percent by our parameter-free potentials. Most discrepancies are comparable with the typical thermal fluctuation of the atomic position at room temperature. The z/c coordinates of O(2) and O(6) of $CsNO_3$(II) have larger discrepancies. However, experiment shows that in $CsNO_3$(II) one O atom in each NO_3 group [O(2), O(6), and O(8), respectively] has a significantly larger thermal ellipsoid than the other O atoms within the same group (18); hence, these discrepancies are still comparable with the thermal fluctuation of the atomic position at room temperature. The lattice constants for the relaxed structure are about 5% shorter than the experimental values, which is a rather general feature for large unit-cell simulations using Gordon–Kim potentials (13). Additionally, the experimental values are room temperature values and thus include the effects of the thermal expansion, while the relaxed lattice is in the ground state and has no temperature effect.

Overall, the comparison of relaxed structures and experimental structures provides a sensitive test of the validity of the theoretical potential energy surfaces. The good agreements of our relaxed structures with the experimental structures indicate that our parameter-free potentials provide

TABLE 1
Theoretical Relaxed Structural Parameters of $RbNO_3$ with $P3_1$ Constraints

Lattice constants:	$a = 10.067$ Å (10.474 Å)	$b = a$	$c = 7.053$ Å (7.443 Å)
Prototype	x/a	y/b	z/c
Rb(1)	0.4570 (0.4474)	0.5667 (0.5575)	0.6343 (0.6483)
Rb(2)	0.1220 (0.1231)	0.2195 (0.2201)	0.0010 (0.0000)
Rb(3)	−0.2243 (−0.2161)	0.2202 (0.2299)	0.6327 (0.6242)
N(1)	0.4590 (0.4612)	0.5859 (0.5915)	0.1593 (0.1628)
N(2)	0.1003 (0.1009)	0.2103 (0.2047)	−0.4768 (−0.4784)
N(3)	−0.2342 (−0.2337)	0.2228 (0.2260)	0.1017 (0.0959)
O(1)	0.4547 (0.4495)	0.6891 (0.6778)	0.2456 (0.2713)
O(2)	0.3781 (0.3927)	0.4534 (0.4597)	0.2118 (0.1935)
O(3)	0.5443 (0.5465)	0.6164 (0.6419)	0.0229 (0.0389)
O(4)	0.0043 (0.0022)	0.1129 (0.1101)	−0.3716 (−0.3799)
O(5)	0.2364 (0.2310)	0.2671 (0.2476)	−0.4387 (−0.4432)
O(6)	0.0589 (0.0637)	0.2498 (0.2519)	−0.6182 (−0.6081)
O(7)	−0.2610 (−0.2729)	0.1431 (0.1458)	0.2427 (0.2269)
O(8)	−0.1024 (−0.1034)	0.3047 (0.3091)	0.0466 (0.0553)
O(9)	−0.3399 (−0.3315)	0.2209 (0.2246)	0.0137 (−0.0015)

Note. Experimental values (Ref. 1) are given in parentheses.

TABLE 2
Theoretical Relaxed Structural Parameters of $CsNO_3$ with $P3_1$ Constraints

Lattice constants:	$a = 10.492$ Å (10.902 Å)	$b = a$	$c = 7.389$ Å (7.74 Å)
Prototype	x/a	y/b	z/c
Cs(1)	0.4490 (0.4481)	0.5581 (0.5557)	0.6464 (0.6527)
Cs(2)	0.1185 (0.1205)	0.2219 (0.2220)	0.0003 (0.0000)
Cs(3)	− 0.2182 (− 0.2161)	0.2248 (0.2282)	0.6353 (0.6333)
N(1)	0.4585 (0.4629)	0.5901 (0.5933)	0.1681 (0.1604)
N(2)	0.1007 (0.1085)	0.2048 (0.2034)	− 0.4769 (− 0.4692)
N(3)	− 0.2336 (− 0.2290)	0.2283 (0.2345)	0.1038 (0.1093)
O(1)	0.4438 (0.4417)	0.6758 (0.6650)	0.2665 (0.2670)
O(2)	0.3873 (0.4004)	0.4581 (0.4650)	0.1978 (0.1673)
O(3)	0.5452 (0.5510)	0.6381 (0.6605)	0.0415 (0.0452)
O(4)	0.0039 (0.0045)	0.1101 (0.1134)	− 0.3823 (− 0.3876)
O(5)	0.2297 (0.2265)	0.2498 (0.2314)	− 0.4393 (− 0.4274)
O(6)	0.0673 (0.0828)	0.2539 (0.2565)	− 0.7071 (− 0.5985)
O(7)	− 0.2576 (− 0.2484)	0.1488 (0.1638)	0.2352 (0.2304)
O(8)	− 0.1076 (− 0.1073)	0.3119 (0.3216)	0.0537 (0.0481)
O(9)	0.3366 (− 0.3311)	0.2239 (0.2231)	0.0207 (0.0210)

Note. Experimental values (Ref. 2) are given in parentheses.

a good representation of the interactions in the alkali nitrates investigated.

MOLECULAR DYNAMICS SIMULATIONS OF THE PHASE TRANSITIONS

Our molecular dynamics simulations started from the theoretical relaxed structures. These simulations follow a constant pressure algorithm (19). Periodic boundary conditions are introduced to simulate an infinite lattice. We used supercells with 360 ions for $RbNO_3$ and $CsNO_3$ which were formed by doubling the hexagonal unit cells in all three directions. At each temperature the averages of the ion positions, energy, etc., were taken over 10 ps using a 1-fs molecular dynamics time step.

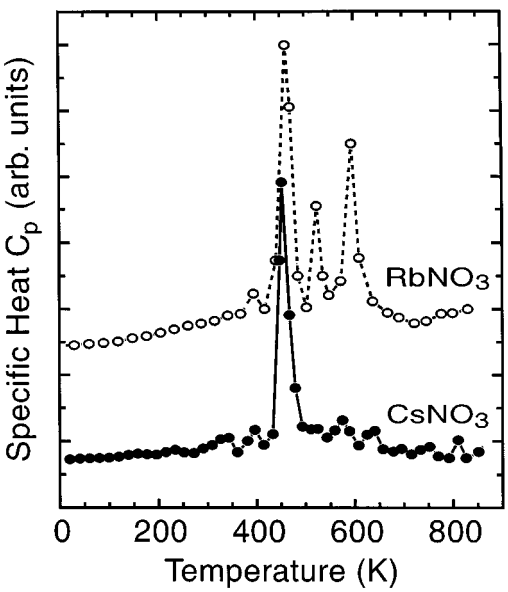

FIG. 1. Specific heat C_p of $RbNO_3$ and $CsNO_3$ as a function of temperature obtained from molecular dynamics "heating."

Figure 1 presents the specific heat as a function of temperature obtained from our simulation for $RbNO_3$ and $CsNO_3$. Three peaks in $RbNO_3$ indicate three phase transitions occurring at 456, 523, and 590 K, respectively, while an anomaly appearing at about 450 K indicates a single phase transition in $CsNO_3$. These theoretical phase transition temperatures are about 5% higher than the experimental values.

We monitor the changes of the projections of average structure along certain directions with temperature. Figures 2–4 show the projections of the ion positions along the [001] (c axis), [101], and [10$\bar{2}$] directions of the hexagonal unit cell in the average structures of the four different phases of $RbNO_3$. The counterparts for $CsNO_3$ are similar to those in Figs. 2a, 2b, 3a, 3b, 4a, and 4b. In the plot the lines connect the nitrogen atoms with the nearest oxygen atoms and the isolated ellipses represent the Rb atoms. Large ovals centered about atoms represent "thermal ellipsoids" which indicate r.m.s. deviation of atoms from their average positions.

a. Disordering Process in IV–III Transition of $RbNO_3$ and II–I Transition of $CsNO_3$

In phase IV of $RbNO_3$ there are three different groups of NO_3 ions whose planes are perpendicular to each other as

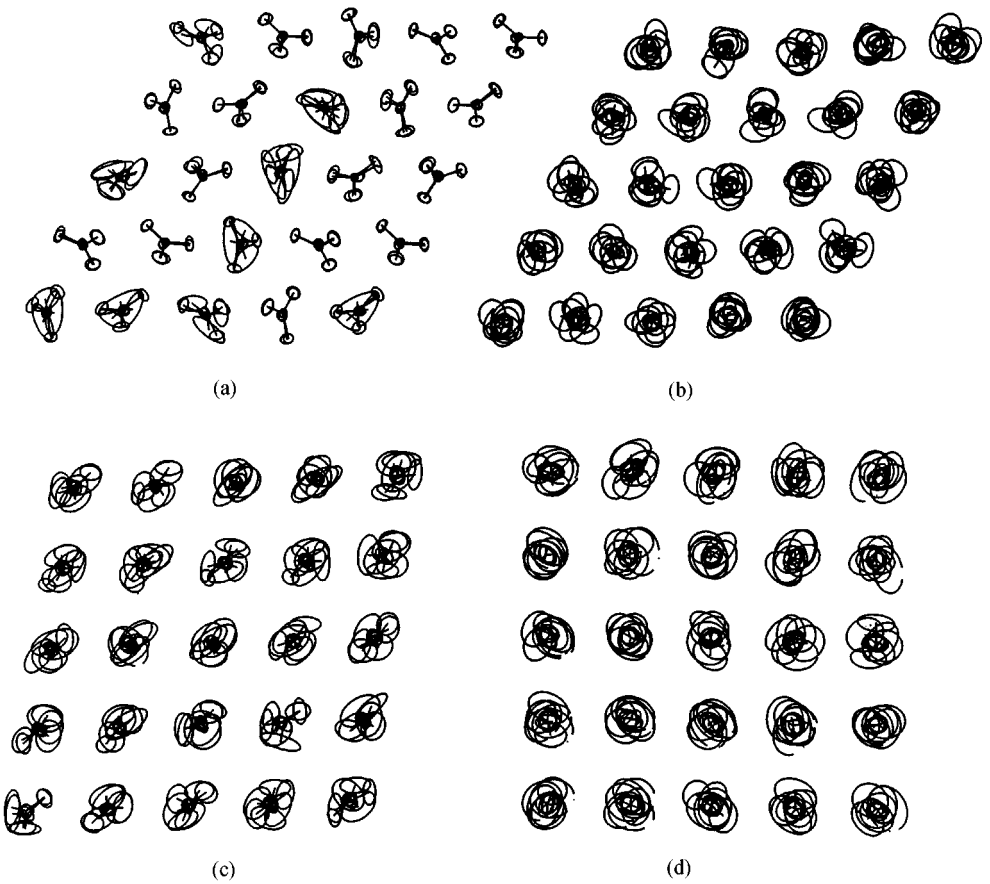

FIG. 2. Projections of the ion positions along the [001] direction (c axis) of the hexagonal unit cell in the average structure of the four different phases of $RbNO_3$ obtained from the MD simulation. (a) Phase IV at 435 K, (b) phase III at 470 K, (c) phase II at 530 K, and (d) phase I at 610 K.

shown in Fig. 3a. We only describe the disordering process of NO_3 ions with planes perpendicular to the [101] direction of the hexagonal unit cell. The orientational distributions $P(\phi)$ of this NO_3 group about the [101] axis and about the $[10\bar{2}]$ axis, an axis parallel to the NO_3 ion planes of this group, are shown in Fig. 5. The NO_3 ions become partially disordered well below the first transition temperature T_{c1}. Some NO_3 ions jump 120° about their triad axes to equivalent sites just above room temperature. Also, 180° out-of-plane jumping about the $[10\bar{2}]$ axis occurs at about the same temperature. This is somewhat surprising as one expects more hindrance to this motion. The orientations of the NO_3 ions become completely random about both axes above the first transition.

The isotropically rotating NO_3 ions are effectively spherical so that the system transforms into a high-symmetry phase with CsCl-type structure (phase III) at T_{c1}. In the process the Rb atoms make small translations to form an ideal cubic sublattice.

X-ray photographs of single crystals heated through the IV–III transformation show that the hexagonal c axis of phase IV transforms to the cubic triad [111] axis of phase III, with the hexagonal [101] direction becoming the cubic [100]-type direction (9). As shown in Figs. 2a, 2b, 3a, and 3b, our simulation reproduces this relationship between phase IV and phase III. Furthermore, from Figs. 4a and 4b we know that the $[10\bar{2}]$ direction of the hexagonal unit cell changes into a [110]-type direction of CsCl structure.

The disordering process of the NO_3 ion during the II–I transition of $CsNO_3$ is the same as that during the phase IV–III transition in $RbNO_3$. The projections of the average structure below and above the T_c are similar to those of $RbNO_3$ shown in Figs. 2a, 2b, 3a, and 3b.

b. III–II–I Transitions in $RbNO_3$

By examination of Figs. 2–4, we find that the phase III–II–I transformations are achieved by a simple differential dilation in which the structure expands along a trigonal axis of phase III and contracts at right angles to this axis. This is illustrated in Fig. 6 and agrees with the models proposed by Salhotra *et al.* (7).

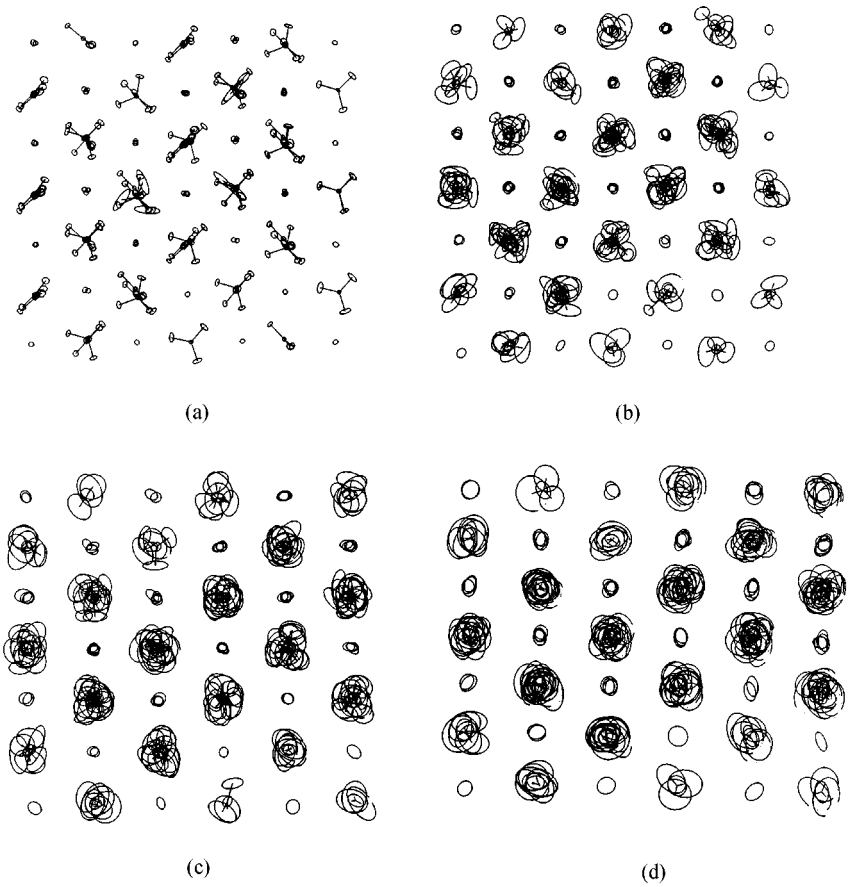

FIG. 3. Projections of the ion positions along the [101] direction of the hexagonal unit cell in the average structure of the four different phases of $RbNO_3$ obtained from the MD simulation. (a) Phase IV at 435 K, (b) phase III at 470 K, (c) phase II at 530 K, and (d) phase I at 610 K.

In detail, there are four [111]-type directions with 3-fold symmetry in phase III (CsCl structure). When the structure transforms from III to II, elongation along one [111]-type direction, whose 3-fold symmetry remains, results in the disappearance of 3-fold symmetry in other three [111]-type directions as shown in Figs. 2b and 2c. Meanwhile, [100]-type directions of phase III lose their 4-fold symmetry because of the dilation along one [110]-type direction and contraction along another [110]-type direction (shown in Figs. 3b and 3c). Three [110]-type directions of phase III transform into three $[0\bar{1}1]$-type directions ($[0\bar{1}1]$, $[10\bar{1}]$, and $[\bar{1}10]$) of rhombohedral structure (Figs. 4b and 4c).

Expansion along the triad axis of phase II continues until the rhombohedral angle becomes 60° and the phase becomes NaCl structure (phase I). From Figs. 2c, 2d, and 6, one can see that three [111]-type directions without 3-fold symmetry of the rhombohedral structure change to three [100]-type directions of the NaCl structure. Three [100]-type directions of phase II become three [110]-type directions of phase I (Figs. 3c and 3d) and three $[0\bar{1}1]$-type directions of phase II change into another three [110]-type directions of phase I (Figs. 4c and 4d).

In the phase III of CsCl structure, the orientation of NO_3 ions has a spherical distribution as shown in Figs. 2b, 3b, 4b, and 5. However, the thermal motions of the NO_3 ions in rhombohedral structure become anisotropic (cf. Fig. 4c). The orientation of the NO_3 ions seems to have a planar distribution, and the normals of all the NO_3 ion planes are along the trigonal axis. The thermal motion of the in-plane rotations is much larger than that of the out-of-plane rotations. This indicates that the rhombohedral phase of $RbNO_3$ has the same structure as the disordered phase of $NaNO_3$, which is in agreement with the result of the neutron powder diffraction (6). The orientation distribution of the NO_3 ions becomes spherical again in the NaCl structure.

The theoretic volume changes during the IV–III–II–I phase transitions are 4.7%, 12.5%, and 3.9%, respectively, which are roughly in agreement with the experimental values of 5.9%, 12.8%, and 4.2% (6).

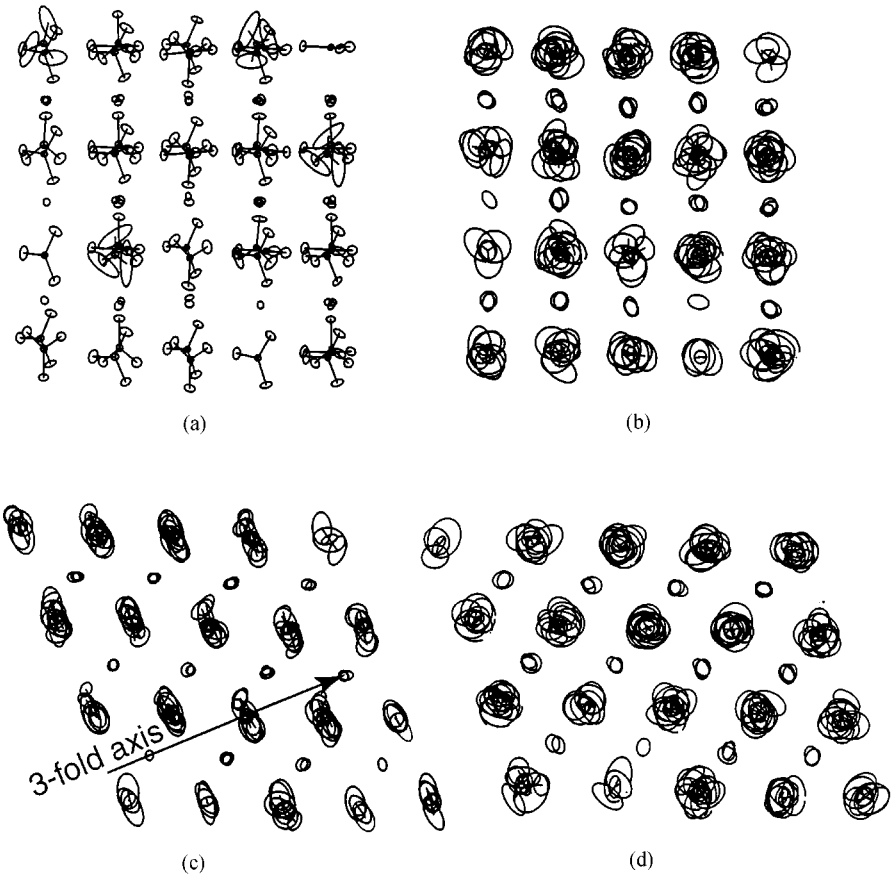

FIG. 4. Projections of the ion positions along the $[10\bar{2}]$ direction of the hexagonal unit cell in the average structure of the four different phases of $RbNO_3$ obtained from the MD simulation. (a) Phase IV at 435 K, (b) phase III at 470 K, (c) phase II at 530 K, and (d) phase I at 610 K.

c. Radial Distribution Functions for Different Phases of $RbNO_3$, and $CsNO_3$

Atom–atom radial distribution functions can provide much information about the structures of our simulated crystals. Figure 7 shows the radial distribution functions for Rb–N, Rb–Rb, and N–N pairs of $RbNO_3$ in four different phases.

The Rb–Rb, Rb–N, and N–N distribution functions in phase IV contain many narrow, sharp peaks, but one can see that Rb and N atoms in phase IV form a distorted CsCl structure although the N atom sublattice has a larger distortion.

The Rb and N atoms construct an ideal CsCl-type structure above the first transition temperature. Thus, the Rb–Rb and N–N distribution are similar, with the corresponding peaks appearing at the same positions. The distance from the first peak to the origin in the Rb–Rb and N–N distribution functions is the lattice constant of the CsCl-type structure, which is 4.39 Å at 470 K compared with the experimental value of 4.37 Å at 453 K (7).

In the CsCl-type structure of phase III, each Rb atom has eight N atoms as its first nearest neighbors; i.e., the coordination number of Rb is eight. When the structure expands along a trigonal axis and transforms to rhombohedral phase II, two N atoms on the triad axis depart from the Rb atom, becoming second nearest neighbors, so the first peak in the Rb–N distribution function of phase III splits into two peaks in phase II. The peaks corresponding to both second and third neighbors in phase III also split into two peaks. The marked changes of peak positions in Rb–N, Rb–Rb, and N–N distribution functions on going from phase III to phase II show that the Rb and N lattices experience reconstruction.

The peak positions of the Rb–N, Rb–Rb, and N–N distribution functions for phase I confirm a face-centered-cubic lattice. The lattice constant equals twice the distance of the first peak from the origin in the Rb–N distribution function. Our theoretical value is 7.20 Å at 610 K, close to the experimental value of 7.32 Å at 563 K (7).

The radial distribution functions for Cs–N, Cs–Cs, and N–N pairs of $CsNO_3$ in phase II and phase I are similar to those of $RbNO_3$ in phase IV and phase III shown in

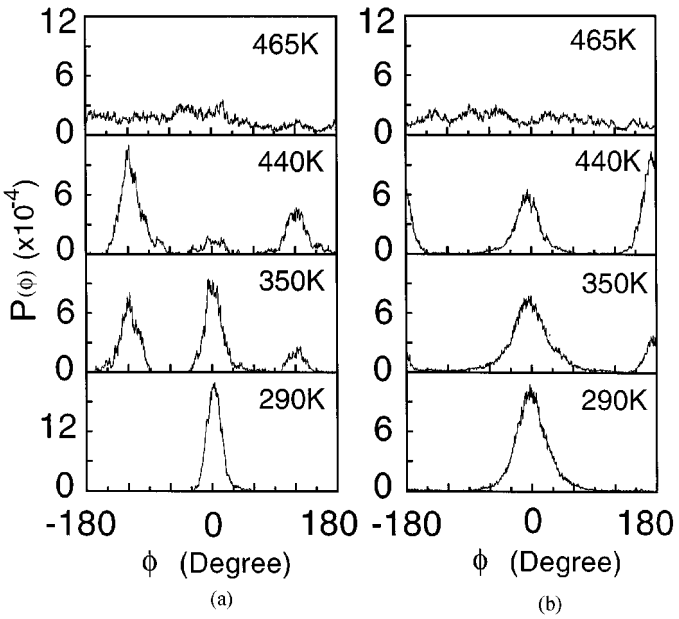

FIG. 5. Orientation distribution $P(\phi)$ of NO_3 ions with planes perpendicular to the [101] direction of the hexagonal unit cell in $RbNO_3$ at different temperatures: (a) about the [101] axis and (b) about [10$\bar{2}$] axis which is axis parallel to the NO_3 planes.

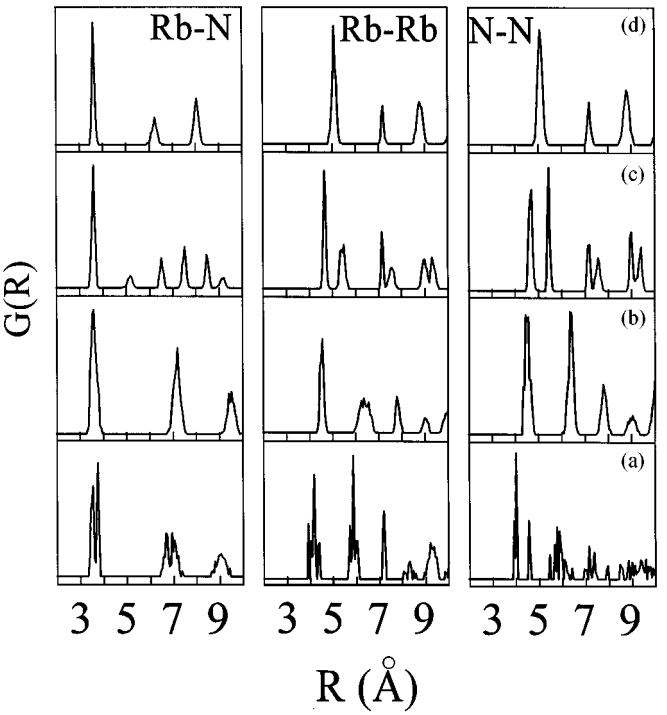

FIG. 7. Atom–atom radial distribution functions for the four different phases of $RbNO_3$: Row (a), phase IV at 435 K; row (b), phase III at 470 K; row (c), phase II at 530 K; and row (d), phase I at 610 K.

Figs. 7a and 7b. Our theoretical lattice constant of phase I obtained from Cs–Cs and N–N distribution functions is $a = 4.50$ Å at 493 K.

DISCUSSION

$RbNO_3$ (III) was established as having a CsCl structure with space group *Pm*3*m* and one molecule per unit cell (4). In order to meet the symmetry requirements of space group *Pm*3*m*, several models of orientational disorder of NO_3 ions have been suggested, which have been reviewed by Shamsuzzoha and Lucas (3). Powder and single-crystal neutron diffraction studies fitted a 12-orientation model of the disorder of the NO_3 ions (4, 6). From our simulation we find that the NO_3 ions in $RbNO_3$(III) and $CsNO_3$(I) are in dynamically disordered states. All the NO_3 ions are performing three-dimensional hindered rotations and the average orientations of the NO_3 ions are random. However, such a hindered rotation of the NO_3 ions is not inconsistent with the 12-orientation model used to refine the neutron diffraction data.

Several authors have discussed the phase III–II–I transformations in $RbNO_3$. Finbak *et al.* (8) indexed the X-ray diffraction powder pattern of phase II as hexagonal and

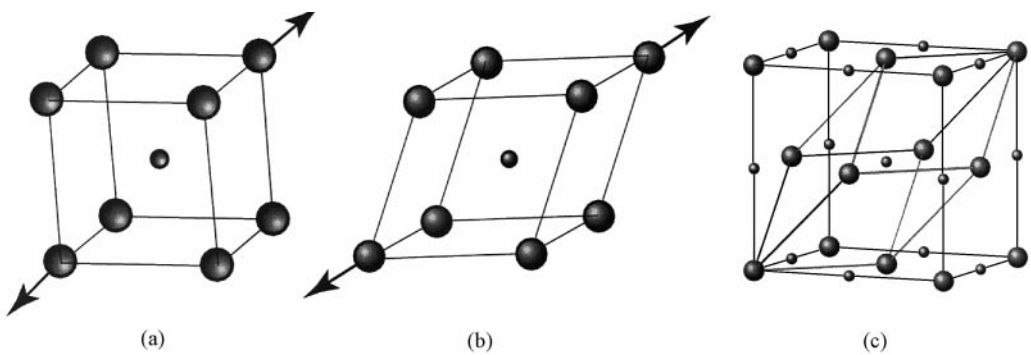

FIG. 6. Structural relationships between (a) phase III (CsCl-type), (b) phase II (rhombohedral), and (c) phase I (NaCl-type). Large circles represent Rb atoms, small circles, N atoms; the arrows indicate the direction of the elongation of the trigonal cell.

gave the corresponding rhombohedral parameters. Brown and McLaren (9) preferred a tetragonal cell for this phase. Salhotra *et al.* (7), based on dilatometric and X-ray diffraction data, confirmed the conclusion of Finbak *et al.* (8) and proposed a mechanism (shown in Fig. 6) for the structural changes at the III–II–I phase transitions. Our simulation results strongly support this model, in which the III–II–I phase transformation is due to a uniaxial extension along the body diagonal of phase III, giving phase II a rhombohedral structure.

Shamsuzzoha *et al.* argued that $RbNO_3$(II) has a b.c.c. lattice with $Z = 8$ (3). The b.c.c. unit cell consists of eight cubic subcells of Rb atoms such that $[100]_{III}//[100]_{II}$ and $2(a)_{III} = (a)_{II}$. This means that phase II is a superlattice of phase III and in phase II the eight NO_3 ions enclosed by the eight cubic subcells of Rb atoms must have different orientations. This situation is unlikely because the orientation of NO_3 ions becomes more disordered at higher temperatures.

ACKNOWLEDGMENTS

This work was supported by the U.S. Army Research Office under Grants Nos. DAAG 55-97-1-0106 and DAAG 55-98-1-0273. The computer facility was supported by Nebraska-E PSCoR-NSF Grant EPS-9720643.

REFERENCES

1. J. Pohl, D. Pohl, and G. Adiwidjaja, *Acta Crystallogr., Sect. B* **48,** 160 (1992).
2. D. Pohl and T. Gross, *Acta Crystallogr., Sect. C* **49,** 316 (1993).
3. M. Shamsuzzoha and B. W. Lucas, *Can. J. Chem.* **66,** 819 (1988).
4. M. Shamsuzzoha and B. W. Lucas, *Acta Crystallogr., Sect. C* **43,** 385 (1987).
5. S. Yamamoto, S. Suematsu, and Y. Shinnaka, *J. Phys. Soc. Jpn.* **43,** 1962 (1977).
6. M. Ahtee and A. W. Hewat, *Phys. Stat. Sol. A* **58,** 525 (1980).
7. P. P. Salhotra, E. C. Subbarao, and P. Wenkateswarlu, *Phys. Stat. Sol.* **29,** 859 (1968).
8. C. Finbak, O. Hassel, and L. C. Stromme, *Z. Phys. Chem. B* **37,** 468 (1937).
9. R. N. Brown and A. C. McLaren, *Acta Crystallogr.* **15,** 974 (1962).
10. M. Shamsuzzoha and B. W. Lucas, *J. Appl. Crystallogr.* **21,** 74 (1988).
11. A. S. Chary, S. N. Reddy, and T. Chiranjivi, *Solid State Ionics* **62,** 293 (1993).
12. R. G. Gordon and Y. S. Kim, *J. Chem. Phys.* **56,** 3122 (1972).
13. H. M. Lu and J. R. Hardy, *Phys. Rev. B* **42,** 8339 (1990).
14. M. J. Frish *et al.*, "GAUSSIAN94." Gaussian, Inc., Pittsburgh, PA, 1994.
15. R. S. Mulliken, *J. Chem. Phys.* **23,** 1833 (1955).
16. E. Clementi and C. Roetti, *At. Data Nucl. Data Tables* **14,** 177 (1974).
17. D. A. Liberman, D. T. Cromer, and J. T. Waber, *Comput. Phys. Commun.* **2,** 107 (1971).
18. B. Lucas, *Acta Crystallogr., Sect. C* **39,** 1591 (1983).
19. M. Parrinello and A. Rahman, *Phys. Rev. Lett.* **45,** 1196 (1980).